JACS
JOURNAL OF THE AMERICAN CHEMICAL SOCIETY

COMMUNICATION

pubs.acs.org/JACS

Irreversible Chemical Reactions Visualized in Space and Time with 4D Electron Microscopy

Sang Tae Park, David J. Flannigan, and Ahmed H. Zewail*

Physical Biology Center for Ultrafast Science and Technology, Arthur Amos Noyes Laboratory of Chemical Physics, California Institute of Technology, 1200 East California Boulevard, Pasadena, California 91125, United States

ABSTRACT: We report direct visualization of irreversible chemical reactions in space and time with 4D electron microscopy. Specifically, transient structures are imaged following electron transfer in copper-tetracyanoquinodimethane [Cu(TCNQ)] crystals, and the oxidation/reduction process, which is irreversible, is elucidated using the single-shot operation mode of the microscope. We observed the fast, initial structural rearrangement due to Cu^+ reduction and the slower growth of metallic Cu^0 nanocrystals (Ostwald ripening) following initiation of the reaction with a pulse of visible light. The mechanism involves electron transfer from TCNQ anion-radical to Cu^+, morphological changes, and thermally driven growth of discrete Cu^0 nanocrystals embedded in an amorphous carbon skeleton of TCNQ. This *in situ* visualization of structures during reactions should be extendable to other classes of reactive systems.

Four-dimensional (4D) ultrafast electron microscopy (UEM) enables studies of structural dynamics with atomic-scale spatial and temporal resolutions.[1,2] Various reversible phenomena have been stroboscopically studied, such as metal−insulator structural dynamics,[3] mechanical vibrations,[4−6] and nanofriction.[7] For irreversible processes, such as ablation,[8] crystallization,[9,10] and phase transitions,[11,12] studies must be made using single-shot imaging. Structures of chemical reactions in the condensed phase, when irreversible, are difficult to probe *in situ* because of the ensuing loss of the material and the thermodynamic stability of the products. However, when imaged in the microscope with the appropriate spatiotemporal resolutions, it is possible to follow both the structural and morphological dynamics in the diffraction patterns and real-space images.

In this communication, we report the 4D visualization of irreversible electron transfer reactions. The processes involved, which include oxidation/reduction, material collapse, and nanocrystal growth, were initiated with a single or multiple optical pulses at a fixed energy, while a single pulse of electrons was used to image the irreversible structural evolution on their nanosecond to millisecond time scales. To characterize changes in structure, images were recorded in three time domains—before, during, and after the reaction—and using 1, 2, ..., N excitation pulses, as shown schematically in Figure 1.

The oxidation/reduction reaction, which leads to the morphological changes and Cu^0 nanoparticle formation, can be

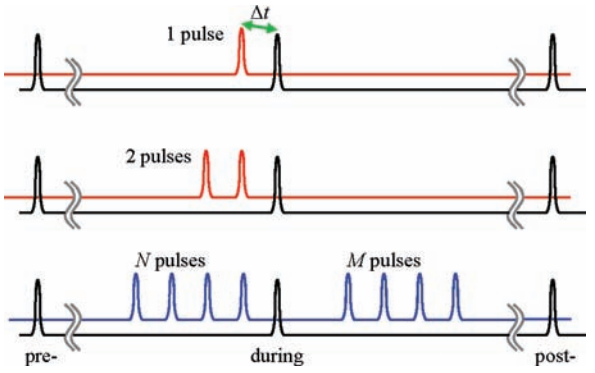

Figure 1. Conceptual diagram of the single-shot experiments. The red (671 nm) and blue (355 nm) solid lines are the optical pulses, whereas the black ones are the probing electron pulses in the *pre*, *during*, and *post*-reaction stage.

expressed by

$$(Cu^+TCNQ^-)_n \xrightarrow{h\nu \text{ or } \vec{E}} Cu^0{}_x + TCNQ^0{}_x + (Cu^+TCNQ^-)_{n-x}$$

This reaction occurs in the quasi one-dimensional structure, and because it can be switched between the reactant (high impedance) and mixed-valence product (low impedance), it is used as a memory material for writing. The reaction can be induced either by an electric field,[13] or by light,[14] but not by thermal heating.[15,16] Previously, we reported studies of the reversible expansion/contraction of Cu(TCNQ) crystals upon irradiation with a train of femtosecond laser pulses at relatively low fluence.[4] The expansion, which is a precursor to crystal collapse and Cu^0 nanoparticle growth, completely recovers on the millisecond time scale.[7] At higher fluences, however, irreversible morphological collapse of the crystal followed by formation and growth of Cu^0 was observed, though the time scales involved were not resolved.

To resolve the irreversible processes associated with oxidation/reduction reactions, the first-generation 4D electron microscope, UEM-1, at the California Institute of Technology was configured in single-shot mode. Details of the UEM-1 instrument and methodology can be found elsewhere.[1,17] In a single-shot mode, the electron pulse is generated with a 266 nm nanosecond laser and contains 2×10^7 electrons, as measured at the detector. The delay between the optical excitation (671 or 355 nm) and electron pulses was controlled with a digital delay generator. For

Received: December 6, 2010
Published: January 21, 2011

ACS Publications © 2011 American Chemical Society

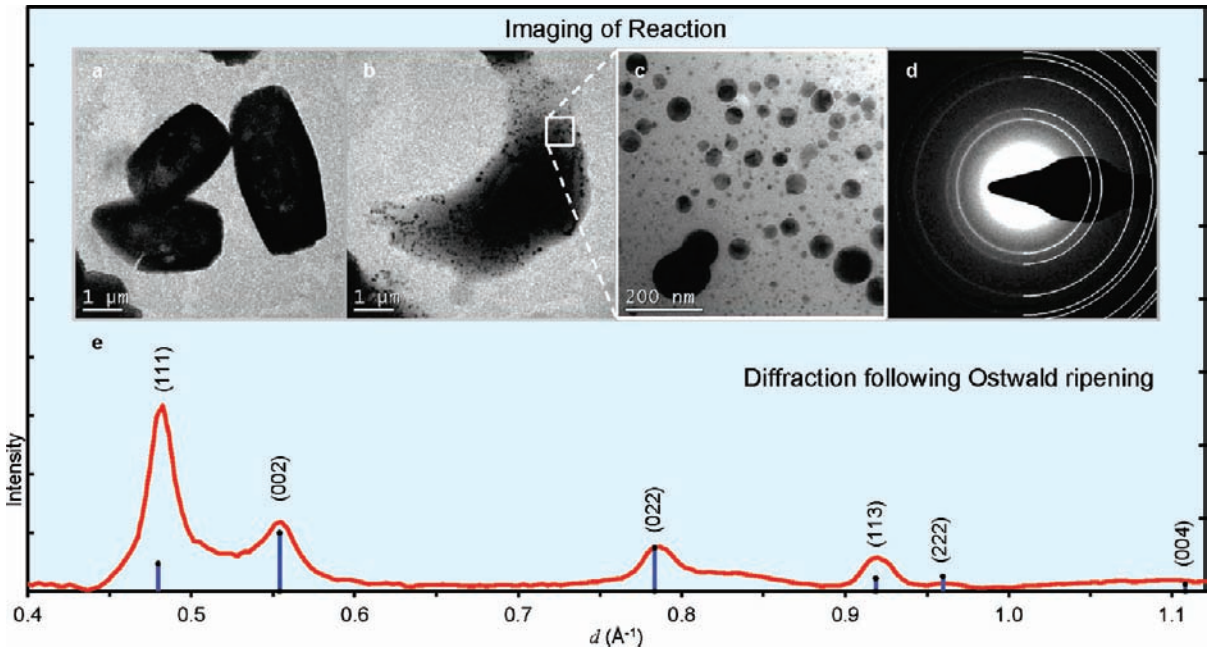

Figure 2. Bright-field images and selected-area electron diffraction of the redox reaction producing Cu^0 nanocrystals. Shown is the evolution from the crystal of Cu(TCNQ) to the metal as evidenced by selected-area diffraction after the nanostructures formed (Ostwald ripening). The images clearly display (a) the initial crystals studied and (b and c) the formation of Cu^0 nanostructures following two pulses of excitation (see Figure 1). (d and e) The diffraction (solid lines in (d) and blue bars in (e) are from the known crystal structure[20]) is that of copper as obtained by Bragg in 1914.

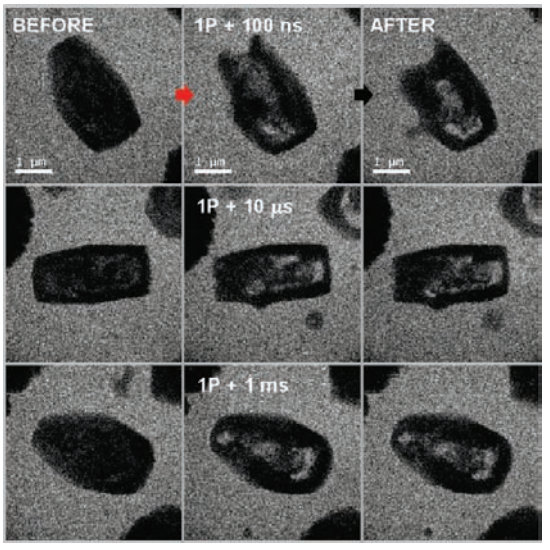

Figure 3. Single-shot images of Cu(TCNQ) single crystals before (first column), at a specific time delay from 100 ns to 1 ms (second column), and several seconds (third column) after exposure to a single laser pulse (671 nm), with which the formation of Cu^0 nanocrystals is not observed. The image labels in the second column denote the time at which the structures were probed after the excitation pulse ($1P + \Delta t$). The arrows in the top row denote the time progression, with red indicating a laser pulse and black indicating only elapsed time of many seconds.

multiple-pulse excitation (i.e., burst mode), a logic circuit (with $\pm$500 ns timing jitter) was built to gate the Q-switch signal in order to select the desired number of pulses. The interval between excitation pulses (80 μs) ensured that the pulse-to-pulse energy remains constant.

The Cu(TCNQ) material is known to display polymorphism; crystals form either a kinetic phase, which shows a needle-like morphology, or a thermodynamic phase, which displays a cube-like morphology.[18] Here, as with our previous work, we exclusively studied the kinetic phase. Single crystals of Cu(TCNQ) were grown directly on a 3×3 array of 20 nm silicon oxide membrane windows, each measuring 100 μm × 100 μm (TEM-windows.com). This was done by reacting a freshly coated 30 nm film of Cu for 5 min with a saturated solution of purified TCNQ (TCI America) in deaerated and dried acetonitrile.[19] For each experiment, care was taken to select single crystals of uniform size and similar local environment in order to minimize possible effects from surrounding material.

Shown in Figure 2 are bright-field TEM images of the single crystals before and after excitation with two pulses of 671 nm laser light. One-pulse excitation results in only partial morphological change, whereas two or more pulses separated by 80 μs induce complete melting with obvious formation of Cu^0 nanocrystals, as determined with higher-magnification imaging (Figure 2c) and selected-area diffraction (Figure 2d,e).

To determine the time scales required for structural changes to occur and Cu^0 nanoparticles to form, we conducted single-shot imaging experiments, whereby temporal snapshots of transient structures of the crystals were obtained after one-pulse (Figure 3) and two-pulse (Figure 4) excitation at 671 nm. For one-pulse excitation, crystal morphological changes occur and are essentially complete within 100 ns. No additional changes are observed thereafter. Further, no noticeable Cu^0 particle formation is seen, regardless of the time at which the reaction is probed. At the same wavelength, when two-pulse excitation was employed (Figure 4), the crystals initially displayed melting, as evidenced by the formation of a viscous, bubbling liquid in less than 10 μs. This was followed by cooling and resolidification and the

dx.doi.org/10.1021/ja110952k | J. Am. Chem. Soc. 2011, 133, 1730–1733

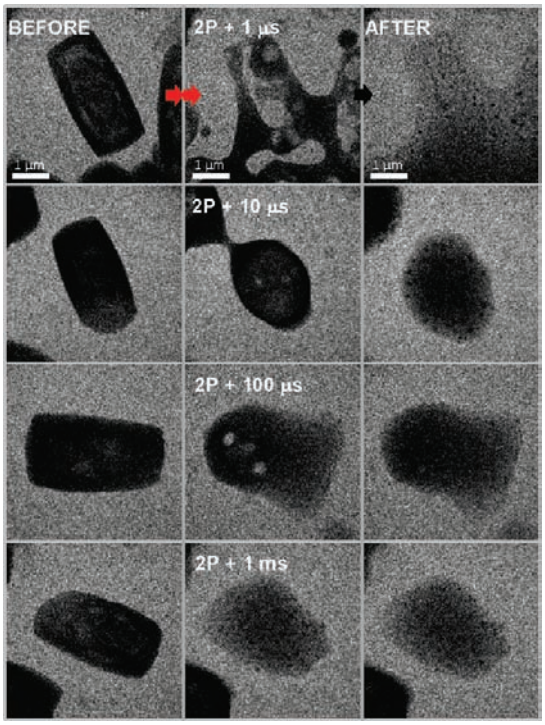

Figure 4. Single-shot images of Cu(TCNQ) single crystals before (first column), at a specific time delay from 1 μs to 1 ms (second column), and several seconds (third column) after exposure to two laser pulses (671 nm), where the formation of Cu^0 nanocrystals is observed, the small dark features in the image. The image labels in the second column denote the time at which the structures were probed after the second excitation pulse ($2P + \Delta t$). The arrows in the top row denote the time progression, with red indicating a laser pulse (in this case, two pulses) and black indicating only elapsed time of many seconds.

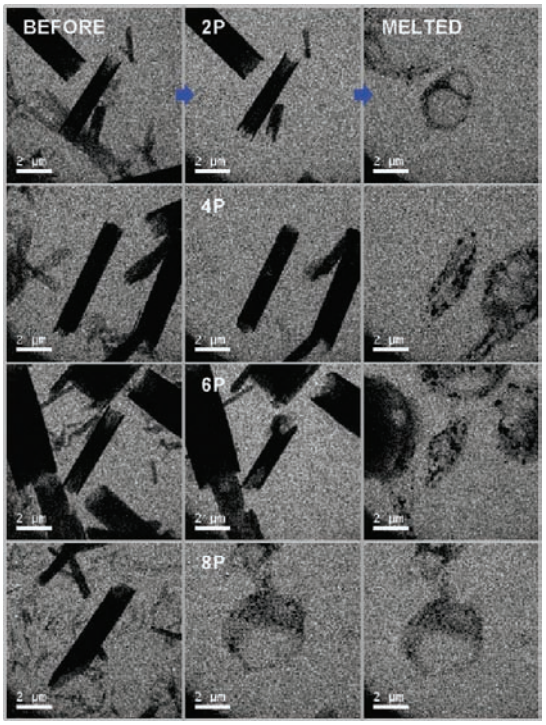

Figure 5. Single-shot images of Cu(TCNQ) single crystals before (first column), and 10 μs after (middle column) a number of (initiation) pulses of 355 nm laser light (120 mJ/cm^2, separated by 80 μs). The third column shows images after additional multiple (finalization) pulses to drive the reaction to completion. The image labels in the second column denote the number of (initiation) pulses.

formation of Cu^0 nanocrystals via sintering and/or Ostwald ripening, all within 1 ms after the second excitation pulse. As shown in Figure 4, these Cu^0 nanocrystals appear in the image as small dark features only after 100 μs.

In contrast to 671 nm, excitation at 355 nm produces different results. Figure 5 shows images of single crystals before and after a number of (initiation) pulses (first and second columns, respectively; see Figure 1). Also shown in the third column are images obtained after the reaction was driven to completion by applying several additional (finalization) pulses after the initial ones. The reaction was deemed complete when no further morphological changes were observed upon application of additional excitation pulses. A gradual shrinking (melting) of the material is observed for excitations with a small number of pulses, while the reaction to form Cu^0 nanocrystals is complete when a train of more than 7 pulses is used. Note, however, that crystals in Figure 5 are larger (and thicker) than those in Figures 3 and 4, and this size difference may at least partially contribute to the observed wavelength dependence.

To quantify the morphological changes and formation of Cu^0 nanoparticles, we obtained the cross correlation of images, that is, the referenced change as a function of the time delay and/or the number of pulses, the results of which reflect the progress of the reaction. As can be visually deduced from Figure 3, we found that the morphological change upon excitation with a single 671 nm pulse is completed in less than 100 ns with no additional changes (i.e., no Cu^0 particle formation) observed beyond this point. When two pulses of 671 nm are used, however, the reaction reaches maturation, indicating the early morphological change is followed by a slower restructuring to form discrete Cu^0 particles. Unlike at 671 nm, the progress of reaction initiated by 355 nm excitation is linearly proportional to the number of pulses and is complete after a minimum of 7 pulses, as can be seen in Figure 5.

From the above results, the mechanism that accounts for the overall reaction and structural changes can now be elucidated. Previous works have shown that exposure of thin films of Cu(TCNQ) to an electric field[13] or to light[14,15] (λ = 458 to 633 nm, and 10.6 μm) results in the formation of a mixed-valence state comprised of a mixture of Cu(TCNQ), neutral TCNQ, and Cu^0. Upon the basis of an apparent insensitivity to the wavelength of light, a mechanism was proposed by which only the electric field is of consequence for the observed redox reaction.[15] Another mechanism, which involves electronic excitations in the TCNQ anion-radical, was proposed. It was suggested that electron transfer may take place from the electronically excited TCNQ anion-radical to Cu^+ due to the lower oxidation potential of the molecular excited state.[16] We note that the reported insensitivity of the reaction to excitation wavelength may indicate the involvement of a low-lying (dark) state as an intermediate.

In our case reported here, because the absorption coefficients are comparable in magnitude at 671 and 355 nm, and both wavelengths correspond to transitions to locally excited states,[21] which will have decreased oxidation potentials relative to the ground state, one may have expected to see no difference in reaction dynamics for excitation at these wavelengths, provided the difference in crystal dimensions (see Figures 4 and 5) do not significantly influence the reactivity. It is therefore possible that our red excitation at 671 nm is to the charge

dx.doi.org/10.1021/ja110952k |*J. Am. Chem. Soc.* 2011, 133, 1730–1733

transfer state between $TCNQ^-$ and Cu^+ and/or that the excitation is dominantly to the intermolecular charge transfer state, as assigned from spectroscopic work, followed by relaxation to the charge transfer from $TCNQ^-$ to Cu^+. We note that independent of the initial excitation, it is clear that this excitation is effective in reducing Cu^+ and the process must involve ligand ($TCNQ^-$) to metal (Cu^+) charge separation.

We have also considered the magnitude of the electric field due to the excitation pulse and the dose level of the electron pulse. The electric field of the laser pulse used here is $\sim 5 \times 10^6$ V/m, which is larger than the previously determined threshold values for the applied DC electric field (1.7×10^5 V/m), and the laser-excitation electric field (6×10^3 V/m).[16] With these fields, the authors did not observe the formation of Cu nanocrystals. Therefore, at our fields, we can observe not only the redox reaction, but also Cu^0 nanocrystal formation. It is worth noting that the exposure of a thin Cu(TCNQ) film to a continuous electron beam having a current of ~ 0.1 μA (0.5 s) results in the formation of Cu^0 particles.[22] We observe no such effect here. While the current can be high in single-pulse UEM imaging (100 μA), the duration of the pulse (in this case 10 ns) is such that irreversible particle formation has insufficient time to occur.[7] Further, the dose delivered to the material in a single-pulse imaging is at least 5 orders of magnitude lower than that in the traditional TEM mode.

Following the Cu^+ reduction, the growth of Cu^0 nanostructures is the result of the process of Ostwald ripening. Once the redox reaction has occurred to form the mixed-valence state, an additional process must take place in order to form the Cu^0 nanoparticles. The redox reaction leads to a significant disruption in the crystal lattice such that expansion occurs.[4,7] Because our excitation pulse energies are significantly above threshold values, residual heat is available to the now unbound Cu^0 atoms in the disrupted lattice. This heat provides the necessary energy for the atoms to rapidly diffuse and coalesce into Cu metal clusters, with an additional driving force provided by a reduction in surface energy. Once the local population density of atoms has fallen below a critical level due to Ostwald ripening, particle growth stagnates. It is known that Cu^0 may initially form smaller structures with different morphologies, depending on the environment.[24−26] These structures were not resolved here, and with UEM further studies should elucidate their transit embryonic nature.

In conclusion, with UEM single-pulse imaging, we have elucidated the spatial and temporal processes associated with a multistep irreversible solid-state chemical reaction. The relevant time scales, which are associated with oxidation/reduction, severe crystal lattice disruption, and the formation of discrete metal nanoparticles, range from nanoseconds to milliseconds. Direct imaging of these processes in real-time, with an observed wavelength dependence, provided new insight into the mechanisms at work in the Cu(TCNQ) quasi one-dimensional material. In general, successful applications of UEM single-pulse imaging to reactive systems opens the door to the study of a wide variety of nanoscale dynamic processes, including sintering and Ostwald ripening, which have significant impacts on, for example, the efficiency of heterogeneous catalytic materials.

AUTHOR INFORMATION

Corresponding Author
zewail@caltech.edu

ACKNOWLEDGMENT

This work was supported by the National Science Foundation and the Air Force Office of Scientific Research in the Physical Biology Center for Ultrafast Science and Technology (UST) supported by the Gordon and Betty Moore Foundation at Caltech.

REFERENCES

(1) Zewail, A. H.; Thomas, J. M. *4D Electron Microscopy: Imaging in Space and Time*; Imperial College Press: London, 2010.
(2) Zewail, A. H. *Science* **2010**, *328*, 187.
(3) Grinolds, M. S.; Lobastov, V. A.; Weissenrieder, J.; Zewail, A. H. *Proc. Natl. Acad. Sci. U.S.A.* **2006**, *103*, 18427.
(4) Flannigan, D. J.; Lobastov, V. A.; Zewail, A. H. *Angew. Chem., Int. Ed.* **2007**, *46*, 9206.
(5) Flannigan, D. J.; Samartzis, P. C.; Yurtsever, A.; Zewail, A. H. *Nano Lett.* **2009**, *9*, 875.
(6) Barwick, B.; Park, H. S.; Kwon, O. H.; Baskin, J. S.; Zewail, A. H. *Science* **2008**, *322*, 1227.
(7) Flannigan, D. J.; Park, S. T.; Zewail, A. H. *Nano Lett.* **2010**, *10*, 4767.
(8) Bostanjoglo, O. In *Advances in Imaging and Electron Physics*; Academic Press, Inc.: San Diego, CA, 2002; Vol. 121, p 1.
(9) Kwon, O. H.; Barwick, B.; Park, H. S.; Baskin, J. S.; Zewail, A. H. *Proc. Natl. Acad. Sci. U.S.A.* **2008**, *105*, 8519.
(10) Taheri, M. L.; McGowan, S.; Nikolova, L.; Evans, J. E.; Teslich, N.; Lu, J. P.; LaGrange, T.; Rosei, F.; Siwick, B. J.; Browning, N. D. *Appl. Phys. Lett.* **2010**, *97*, 032102.
(11) LaGrange, T.; Campbell, G. H.; Turchi, P. E. A.; King, W. E. *Acta Mater.* **2007**, *55*, 5211.
(12) Park, H. S.; Kwon, O. H.; Baskin, J. S.; Barwick, B.; Zewail, A. H. *Nano Lett.* **2009**, *9*, 3954.
(13) Potember, R. S.; Poehler, T. O.; Cowan, D. O. *Appl. Phys. Lett.* **1979**, *34*, 405.
(14) Potember, R. S.; Poehler, T. O.; Benson, R. C. *Appl. Phys. Lett.* **1982**, *41*, 548.
(15) Potember, R. S.; Hoffman, R. C.; Benson, R. C.; Poehler, T. O. *J. Phys. (Paris)* **1983**, *44*, 1597.
(16) Kamitsos, E. I.; Risen, W. M. *J. Chem. Phys.* **1983**, *79*, 5808.
(17) Lobastov, V. A.; Srinivasan, R.; Zewail, A. H. *Proc. Natl. Acad. Sci. U.S.A.* **2005**, *102*, 7069.
(18) Heintz, R. A.; Zhao, H. H.; Xiang, O. Y.; Grandinetti, G.; Cowen, J.; Dunbar, K. R. *Inorg. Chem.* **1999**, *38*, 144.
(19) Melby, L. R.; Mahler, W.; Mochel, W. E.; Harder, R. J.; Hertler, W. R.; Benson, R. E. *J. Am. Chem. Soc.* **1962**, *84*, 3374.
(20) Bragg, W. L. *Philos. Mag.* **1914**, *28*, 355.
(21) The absorption spectrum[16,22] of Cu(TCNQ) shows broad features at $\sim$2100 and 700 nm. The former, which depends on crystallite size, is assigned as an intermolecular ($TCNQ^-$ to neighboring $TCNQ^-$) charge-transfer band to form neutral TCNQ and $TCNQ^{2-}$, and the latter is due to a locally excited state of the $TCNQ^-$ moiety, $^2B_{2g} \rightarrow {}^2B_{1u}{}^{(1)}$ (long axis polarized).[16,22,23] Strong absorption around 400 nm is also observed and is due to overlapping transitions, $^2B_{2g} \rightarrow {}^2B_{1u}{}^{(2)}$ (long axis polarized) and $^2B_{2g} \rightarrow {}^2A_u$ (short axis polarized).
(22) Kamitsos, E. I.; Papavassiliou, G. C.; Karakassides, M. A. *Mol. Cryst. Liq. Cryst.* **1986**, *134*, 43.
(23) Tanaka, J.; Tanaka, M.; Kawai, T.; Takabe, T.; Maki, O. *Bull. Chem. Soc. Jpn.* **1976**, *49*, 2358.
(24) Gronbeck, H.; Broqvist, P. *Phys. Rev. B* **2005**, *71*, 073408.
(25) Curtis, A. C.; Duff, D. G.; Edwards, P. P.; Jefferson, D. A.; Johnson, B. F. G.; Kirkland, A. I.; Wallace, A. S. *J. Phys. Chem.* **1988**, *92*, 2270.
(26) Anderson, P. A.; Edmondson, M. J.; Edwards, P. P.; Gameson, I.; Meadows, P. J.; Johnson, S. R.; Zhou, W. Z. *Z. Anorg. Allg. Chem.* **2005**, *631*, 443.